LETTER

Analysis and Design of Wide-Band Digital Transmission in an Electrostatic-Coupling Intra-Body Communication System

Yuhwai TSENG[†*a)], **Chauchin SU**[††b)], *Nonmembers, and* **Chien-Nan Jimmy LIU**[†c)], *Member*

SUMMARY This study develops a form of digital baseband Intra-Body communication for wideband transmission. A simplified circuit model of signal and noise is constructed to analyze the contribution of the high pass filter function of the electrostatic coupling Intra-Body communication system to wideband digital transmission in electrostatic coupling Intra-Body communication. A unit step function is presented to determine the maximum high pass 3 dB pole that can ensure favorable signal quality in a baseband Intra-Body communication system. Body noise is measured to estimate the range of the high pass 3 dB pole with good Signal to Noise Ratio. A 3.3 Volt battery-powered FPGA is experimentally implemented to confirm the feasibility of the wideband Intra-Body communication system. The experimental results indicate that the digital baseband Intra-Body communication system supports a data rate of more than 16MPS.

key words: *Intra-Body communication, body network, wideband transmission*

1. Introduction

Intra-body commutation (IBC) is a new wireless technique that can integrate electronic devices located discretely on individuals such as mobile phones, PDAs, wearable computers, and biomedical sensors and actuators, all of which use the human body as a transmission media. IBC systems are divided into two categories, *electrostatic coupling* (ESC) and *electromagnetic waveguide* (EMW) systems. By using an electrode to couple the signal into the human body, the ESC IBC system is not grounded since the other electrode is kept open; the environment is used as the signal return path. Meanwhile, an EMW system generates electromagnetic waves using two electrodes, and regards the human body as a waveguide to transmit the signal.

The ESC IBC system proposed in [1]–[3] transmit and receive data using the conventional RF modulation approach and electrode sensors applied on the human body. The data rate of the proposed ESC IBC system is limited to 417 kbits per second (BPS) [2] since the lack of the same ground between the transmitter and the receiver degrades the signal quality, especially for a low frequency signal. Nipon Telegraph and Telephone Corporation (NTT) [4] developed an expensive electric-field conversion sensor that comprised of electro-optic crystals and laser light to replace the conventional electrode sensor in order to improve the system data rate to 10M BPS. A recent study [5] devised a digital baseband transceiver of the ESC IBC system by utilizing a complex analogue and digital circuit design procedure under the situation of the poor signal quality in order to increase the system data rate to 2M BPS.

Based on the digital baseband transmission scheme, this work presents an effective means for designing a wideband ESC IBC system by simply altering the load resistor R_L in front of the receiver that offers a high data rate and low power consumption and simplified circuit design. A simplified signal and noise circuit model of the human body is developed to analyze the properties of the signal and noise in the ESC IBC system. The maximum system *high pass* 3 dB *pole* (P_{h3dB}) is derived using the unit step function to provide the system with favorable signal quality. Simulation results indicate that a load resistor R_L which corresponds to the optimum P_{h3dB} under the maximum system P_{h3dB} can maintain a high system SNR. Additionally, conventional electrode sensors are implemented to connect the human body directly to the transmitter and receiver. The experimental results demonstrate the feasibility of the proposed approach.

The rest of the paper is organized as follows. Section 2 proposes the circuit model of the signal and noise respectively in an ESC IBC system. Section 3 elucidates the unit step response of the system P_{h3dB} to the transmission of a baseband digital signal. Section 4 presents the results of system simulation and SNR estimation. Section 5 presents the experimental setup and results. Finally, Sect. 6 draws conclusion.

2. Model of Signal and Noise in ESC IBC System

2.1 Signal and Noise Model

The characteristic of the body tissue can be represented by a time constant circuit which is composed of resistance and capacitance [6]–[8]. Hence, the human body can be model as an equivalent circuit of resistance and capacitance. Biomedical engineers generally view the human body as a resistor network [7]–[10]. The body capacitance is neglected in the body network since the signals that can be

Manuscript received June 18, 2009.
Manuscript revised July 27, 2009.

[†]The authors are with the Electrical Engineering Department, National Central University, No.300, Jung-Da Rd., Jhong-Li City, Taiwan 320, R.O.C.

[††]The author is with the Department of Electrical and Control Engineering, National ChiaoTung University, No.1001, Ta-Hsueh Rd., Hsin-Chu City, Taiwan 300, R.O.C.

[*]Corresponding author.

a) E-mail: s0541004@cc.ncu.edu.tw
b) E-mail: ccsu@cn.nctu.edu.tw
c) E-mail: jimmy@ee.ncu.edu.tw

DOI: 10.1587/transcom.E92.B.3557

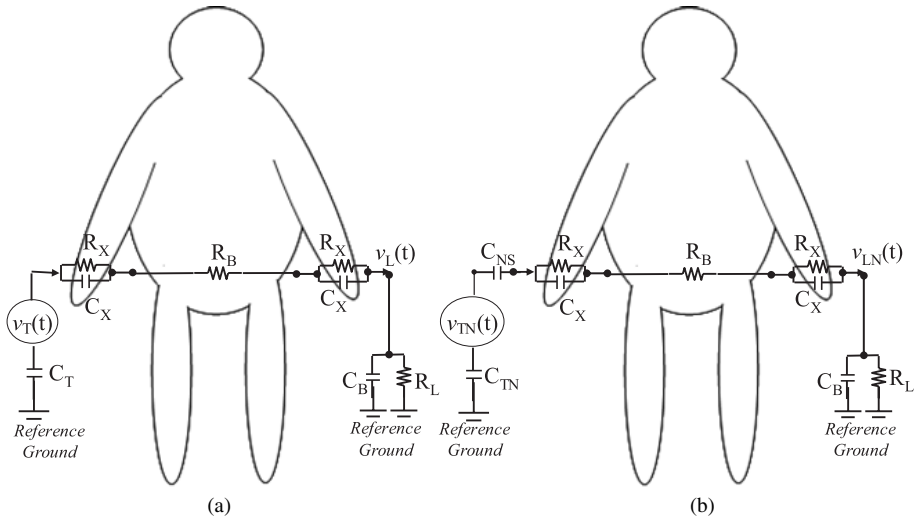

Fig. 1 Signal and noise circuit model of the ESC IBC system (a) Signal (b) Noise.

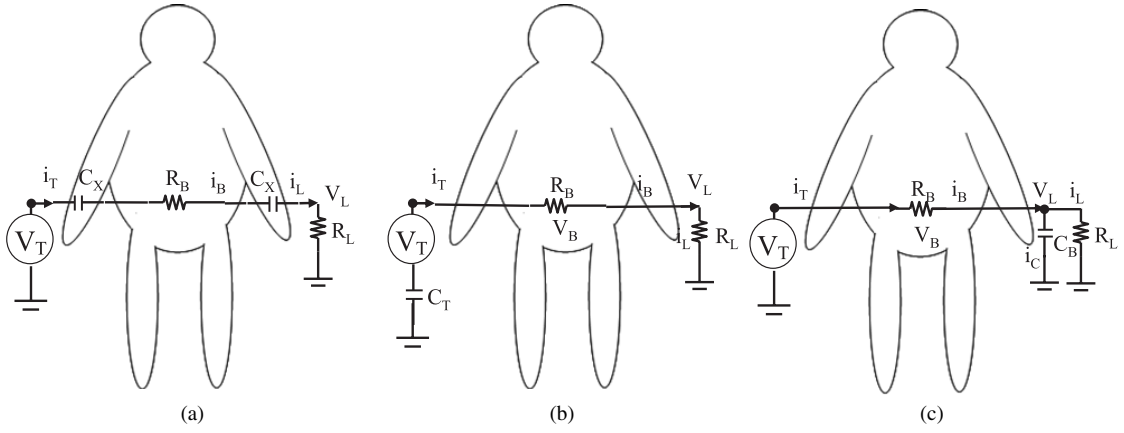

Fig. 2 (a) Simplified model for R_B and C_X measurement. (b) Simplified model for C_T measurement. (c) Simplified model for C_B measurement.

passed through the body network are low frequency biomedical signals, such as ECG, EEG, and EMG. In [1], [2], the signals transmitted through the human body are high frequency data. However, exactly how the body resistance affects the body network has been neglected. The human body can be modeled as a capacitor network. Since a wideband signal are transmitted in the human body, including low and high frequency ones, the body resistance and capacitance should be considered in designing the digital baseband ESC IBC system.

Figure 1 presents a simplified signal and noise circuit model of the ESC IBC system for the baseband signal transmission. Figure 1(a) depicts a signal model that consist of a transmitter with output $v_T(t)$ and a receiver with a load resistor R_L and an input of $v_L(t)$. Figure 1(b) illustrates a noise model that has a noise source $v_N(t)$, receiver front end input $v_{LN}(t)$, and capacitor C_{NS}, which couples noise from $v_{TN}(t)$ to the human body. The human body is modeled as a simplified circuit that is replaced by skin resistance R_X, skin capacitance C_X, and a body resistance R_B. Suppose that the ground of the receiver is the reference ground. Where C_T and C_{TN} denote the ground return-path of the transmitter and noise source respectively; C_B represents the capacitance from the body to the ground and C_{NS} refer to the capacitor from the noise source to the body.

Typical values of C_T, C_{TN}, C_{NS} and C_B are in the pF range and C_X is in nF range, i.e. a thousand times less than C_T and C_B. $X_{CT} \gg X_{CB}(X_{CT} = |\frac{1}{j\omega C_T}|, X_{CB} = |\frac{1}{j\omega C_B}|)$. Therefore,the contributions of skin resistance R_X and skin capacitance C_X to the system are neglected. The transfer function of the signal and noise model can be simplified as Eqs. (1) and (2), respectively.

$$H(s) = \frac{V_L(s)}{V_T(s)} = \frac{s}{R_B C_B(s^2 + 2\zeta\omega_n s + \omega_n^2)}. \quad (1)$$

$$H_N(s) = \frac{V_{LN}(s)}{V_N(s)} = \frac{s}{R_B C_B(s^2 + 2\zeta_N\omega_{nN} s + \omega_{nN}^2)}. \quad (2)$$

Where $\omega_n = \sqrt{\frac{1}{R_B R_L C_T C_B}}$, $\omega_0 = \frac{1}{R_B C_B} + \frac{1}{R_B C_T} + \frac{1}{R_L C_B}$, $\zeta = \frac{\omega_0}{2\omega_n}$ for the signal model and $\omega_{nN} = \sqrt{\frac{1}{R_B R_L C_N C_B}}$, $\omega_{0N} =$

$\frac{1}{R_B C_B} + \frac{1}{R_B C_N} + \frac{1}{R_L C_B}$, $\zeta_N = \frac{\omega_{0N}}{2\omega_{nN}}$ ($C_N = \frac{C_{TN} C_{NS}}{C_{TN}+C_{NS}}$) for the noise model. Equations (1) and (2) are band pass functions with a high pass 3 dB pole (P_{h3dB}, P_{h3dBN}) and a low pass 3 dB pole (P_{l3dB}, P_{l3dBN}) as follow.

$$H(s) \rightarrow \begin{cases} P_{h3dB} = \omega_n \varsigma \left(1 - \sqrt{1 - \frac{1}{\varsigma^2}}\right) \ldots (a) \\ P_{l3dB} = \omega_n \varsigma \left(1 + \sqrt{1 - \frac{1}{\varsigma^2}}\right) \ldots (b) \end{cases}. \quad (3)$$

$$H_N(s) \rightarrow \begin{cases} P_{h3dBN} = \omega_{nN} \varsigma_N \left(1 - \sqrt{1 - \frac{1}{\varsigma_N^2}}\right) \ldots (a) \\ P_{l3dBN} = \omega_{nN} \varsigma_N \left(1 + \sqrt{1 - \frac{1}{\varsigma_N^2}}\right) \ldots (b) \end{cases}. \quad (4)$$

2.2 Determination of the Model Parameters

Equations (1) and (2) indicate that both the signal and noise model of the human body are the bandpass system. Varying R_L can transform the bandpass system into a high pass or low pass system. By assuming that $C_T = C_{TN}$, this work evaluates C_{NS} by applying an estimation method proposed elsewhere [9]. By properly selecting R_L and frequency band, the values of R_B, C_X, C_B, and C_T are characterized in the following means.

High pass transfer function determining R_B, C_X and C_T

Under the condition of same ground between the transmitter and receiver, enabling selection of a frequency and a load R_L such that $R_X \gg X_{CX}$ and $X_{CB} \gg R_L$ (where $X_{CX} = |\frac{1}{sC_X}|$). Now, R_X and X_{CB} can be neglected. Figure 1(a) can be simplified as Fig. 2(a), in which the bandpass system transfer function becomes a high pass transfer function expressed as

$$H(s) \cong \frac{R_L}{R_B + R_L} \times \left(\frac{s}{s + \frac{2}{(R_B + R_L) \times C_X}} \right). \quad (5)$$

In this case, $R_L = 25\,\Omega$; $f \gg 600\,\text{kHz}$ is in the pass band of the high pass system and $f < 265\,\text{kHz}$ is in the stop band of the high pass system. When $f \gg 600\,\text{kHz}$, R_B can be derived as

$$R_B \cong R_L \times \left(\left| \frac{V_T(j2\pi f)}{V_L(j2\pi f)} \right|_{f \gg 600K} - 1 \right). \quad (6)$$

With R_L known and $v_L(t)$ measured, the current flow from the transmitter through the body to the receiver can be determined. Additionally, C_X can be derived in the stop band of the high pass system as

$$C_X \cong \frac{2 \times |I_L(j2\pi f)|}{2\pi f \times [|V_T(j2\pi f)| - |V_L(j2\pi f)| - |I_L(j2\pi f)| \times R_B]_{f<265\,kHz}}. \quad (7)$$

C_T is evaluated under the ground-free condition. Since $C_X \gg C_B \gg C_T$, we are able to increase the signal frequency and decrease R_L to have $X_{CX} \ll R_B$ and $R_L \ll X_{CB}$. The model is simplified to the one shown in Fig. 2(b). Equation (1) becomes a high pass transfer function. In this case, $R_L = 25\,\Omega$; $f < 2\,\text{MHz}$ is in the stop band of the high pass system. C_T can then be derived in the stop band of the high pass system as

Table 1 C_{NS}, R_B, C_X, C_B, and C_T measuring parameters and results.

	R_L (Ω)	Evaluation Frequency Range	Test square waveform f_S	Left Wrist To Right Wrist
C_{NS}	1M	60Hz		$8.2pf$
R_B	25	600KHz~800KHz	5KHz	440Ω
C_X	25	65KHz~265KHz	5KHz	$25nF$
C_B	10K	3MHz~7MHz	100KHZ	$79pF$
C_T	25	1.2MHz~2MHz	20KHz	$2.85pF$

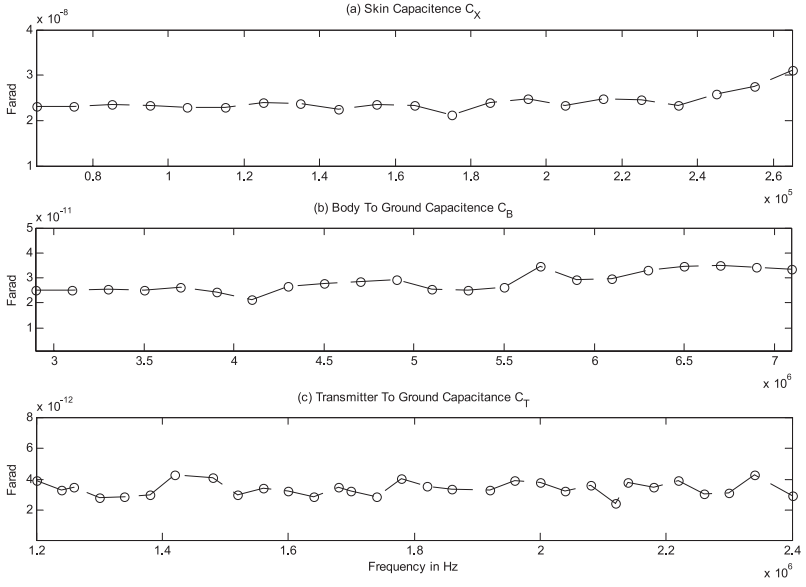

Fig. 3 Evaluated result of model parameters.

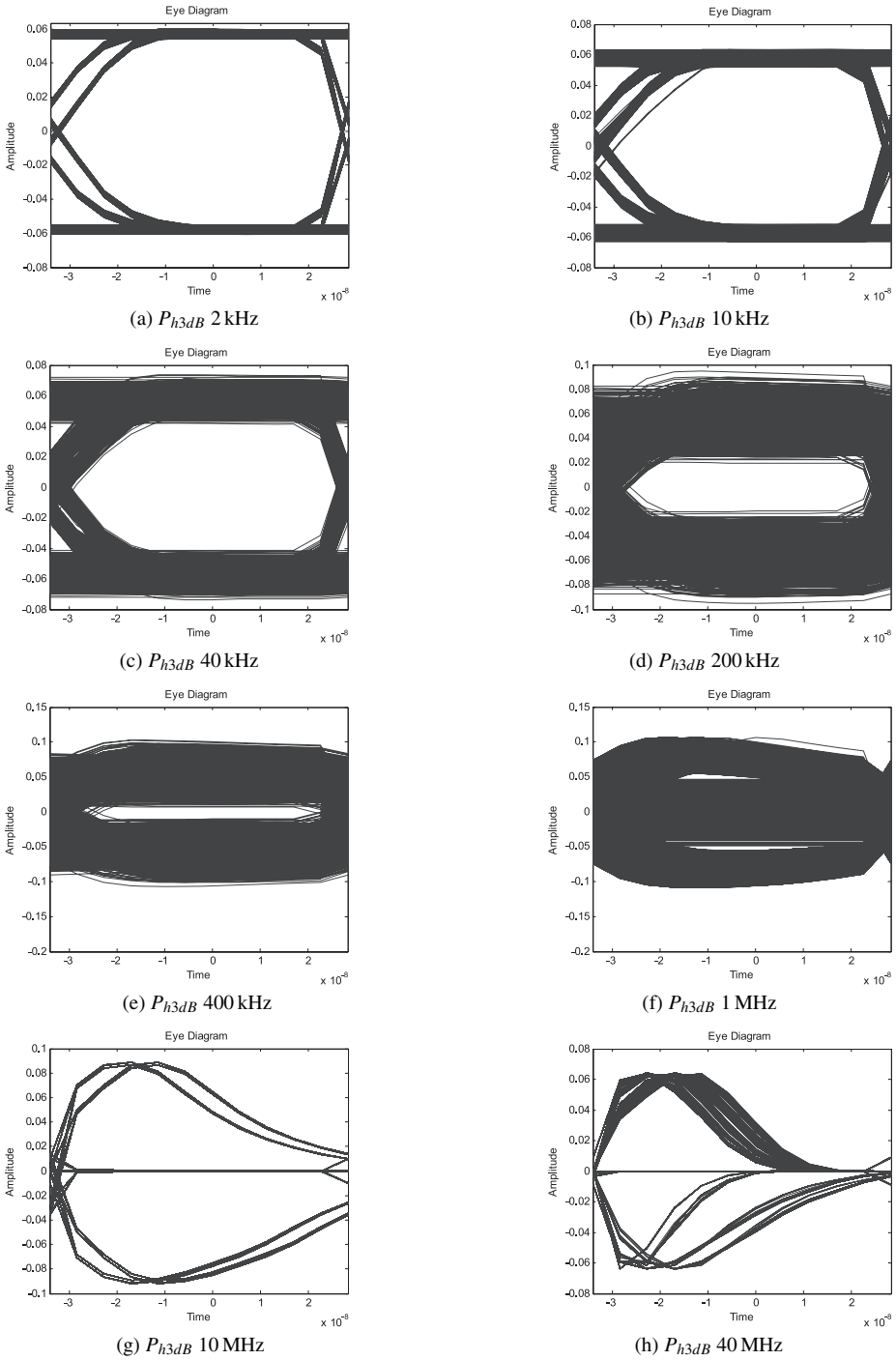

(a) P_{h3dB} 2 kHz (b) P_{h3dB} 10 kHz

(c) P_{h3dB} 40 kHz (d) P_{h3dB} 200 kHz

(e) P_{h3dB} 400 kHz (f) P_{h3dB} 1 MHz

(g) P_{h3dB} 10 MHz (h) P_{h3dB} 40 MHz

Fig. 4 Eye diagrams of the simulation output $v_T(t)$ with various P_{h3dB}.

$$C_T \cong \frac{|I_L(j2\pi f)|}{2\pi f \times [|V_T(j2\pi f)| - |V_L(j2\pi f)| - |I_L(j2\pi f)| \times R_B]_{f<2\,MHz}}. \quad (8)$$

Low pass transfer function determining C_B

Similarly, a frequency and a load resistor R_L can be found such that $X_{CB} \ll R_L$. The circuit model becomes the one shown in Fig. 2(c), in which the bandpass system transfer function becomes a low pass transfer function. In this case, $R_L = 10\,\mathrm{k}\Omega$; $f \gg 3$ MHz is in the stop band of the low pass system. Since $i_T(t) = i_B(t) = i_{CB}(t) + i_L(t)$, C_B is derived in the stop band of the low pass system as

$$C_B \cong \frac{1}{2\pi f \times |V_L(j2\pi f)|} \times \left[\frac{|V_T(j2\pi f)|}{R_B} - \frac{|V_L(j2\pi f)|}{R_L // R_B}\right]_{f \gg 3\,MHz}. \quad (9)$$

Table 1 lists C_{NS}, R_B, C_X, C_B, and C_T evaluating parameters and results. Figure 3 shows the evaluation results

of the related capacitances C_X, C_B and C_T from the left wrist to the right wrist with a distance of 1.5M. The measured human body is 1.75M in height and 70 kg in weight. Due to noise effect and circuit simplification, the measured results are not constant in the specific frequency range. The values given in Table 1 are the averaged results of the specific frequency band of the specific frequency band.

3. Unit Step Response of System High Pass Pole to Digital Signal Transmission

Equation (1) presents the transfer function of human body channel. It is band pass filter function. This work neglects the contribution of P_{l3dB} to the system since $P_{l3dB} \cong 132$ MHz is greater than P_{h3dB}. The effect of the P_{h3dB} in the system on the digital baseband signal transmission weakens the transmitted signal, especially when 1 or 0 data are repeatedly transmitted.

To ensure favorable signal quality, this work proposes the use of a unit step function to determine the maximum P_{h3dB} of the system. The unit step function $u(t) - u(t - nT_b)$ represents the transmission of "1"s with duration T_b n times by the transmitter. From the circuit model in Fig. 1 and Eq. (1), the output of the system is the convolution operation of the unit step function $u(t) - u(t - nT_b)$ with $h(t)$ in time domain, as shown in below.

$$[u(t) - u(t - nT_b)] \otimes h(t) = \frac{V}{R_B C_B 2\omega_n \zeta \sqrt{1-\frac{1}{\zeta^2}}} \left(e^{-P_{h3dB}t} - e^{-P_{h3dB}(t-nT_b)}u(t-nT_b)\right). \quad (10)$$

This study defines R_{EM} as the minimum energy reserve ratio in the system at data transition time $t = nT_b$. R_{EM} is obtained by dividing $u(t) \otimes h(t)$ by $u(t - nT_b) \otimes h(t)$.

$$R_{EM} \le e^{-P_{h3dB}nT_b} \quad t \ge nT_b. \quad (11)$$

For the desirable n and R_{EM} level, the maximum P_{h3dB} of the system is as follows.

$$P_{h3dB} \le -\frac{\ln(R_{EM})}{n} f_b. \quad (12)$$

where f_b represents the data rate of the system. Equation (12) indicate that a higher R_{EM} and n result on a lower P_{h3dB} and good signal quality.

4. Simulation of the System and Estimation of SNR

This study utilizes the Hspice Circuit Simulator to simulate the simplified body circuit model that is presented in Fig. 1(a) and the corresponding parameters are presented in Table 1. The input data $v_T(t)$ are 60000 bits of PRBS (Pseudo-Random Binary Sequence) data with maximum length 21 delivered at a rate of 16M BPS and an output voltage 3.3 V. The body output data $v_L(t)$ are then obtained. In this work, n is 21 and f_b is 16 MHz, in which the desirable

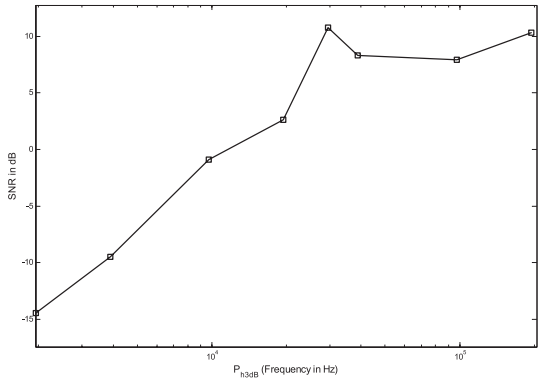

Fig. 5 Estimated SNR with various P_{h3dB}.

R_{EM} level is 0.75; hence the maximum P_{h3dB} of the simulation system (which is evaluated from Eq. (12)) is 220 kHz. To estimate SNR of the system, this study also measures the body noise, using an Agilent 54382D mixed-signal oscilloscope.

Figure 4 present eye diagrams of the simulated receiver output $v_T(t)$ for various P_{h3dB}. These eye diagrams reveal that a lower P_{h3dB} in the system transfer function corresponds to more open white space in the eye diagrams, and the higher signal quality of the system.

The estimated SNR compares the simulation data with the measured body noise, as shown in Fig. 5. The result indicates that the SNR is better than 8 dB when P_{h3db} is between 30 kHz and 200 kHz. The lower P_{h3dB} is associated with a wider bandwidth of the low frequency noise, and the SNR becomes poorer when P_{h3db} is below 30 kHz.

5. Experimental

Figure 6 presents the experimental architecture of the digital wideband intra-body transmission system. The system comprises a transmitter, a receiver and human body channel. The transmitter and the receiver adopt a different battery power to imitate the ESC IBC system operating in the environment of the ground free. The stainless steel electrodes connect the human body to both the transmitter and the receiver. The transmitting distance between the transmitter and the receiver is 1.5 m away from the left wrist to the right wrist which has the same condition as that shown in Fig. 1(a) and Table 1.

The transmitter, which was implemented using Xilinx Spartan II E FPGA development Kit is a pseudorandom data generator consisting of m-sequence linear feed back shift register with a length of 22 and output voltage of 3.3 V with a power consumption of 560 μW. The system data rate is 16M BPS, and n is 21. The maximum P_{h3dB} of the experimental system is 220 kHz as calculated from Eq. (12), i.e. the same as the simulation system described in Sect. 4.

The receiver components consist of a front-end amplifier, R_1 (56 kΩ) and R_2 (10 kΩ) which provide the bias voltage to the front-end amplifier, capacitor C_L (100 nf) which isolates the DC current flow into the human body. The front-

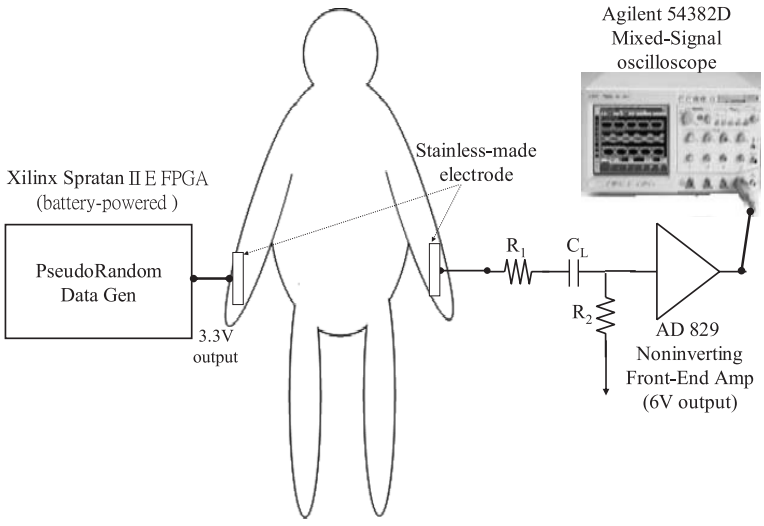

Fig. 6 Block diagram of the experimental set up.

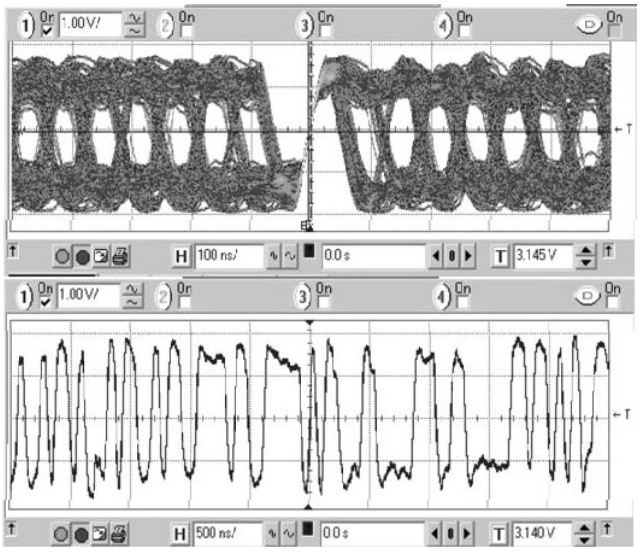

Fig. 7 Implemented system output data — Eye diagram and typical waveform.

end amplifier is a cascade noninverting amplifier made by OPAMP AD829 with gain 24. A series combination of resistors R_1 and R_2 provides the optima P_{h3dB} of 30 kHz to the system that have a higher SNR, which is the same as that shown in Fig. 5.

An Agilent 54382D Mixed-Signal oscilloscope connects to the front-end amplifier in order to measure the output signal of the body. Figure 7 displays an eye diagram and a typical waveform of the front-end amplifier output. As described in Sect. 2 and Fig. 1, the experimental results reveal that the various load resistors R_L will degrade the amount of the signal and the noise simultaneously, and by properly selecting the load resistor R_L can reduce the amount of the noise to increase the system SNR.

The eye diagram includes a 1.5 V white space which is 50% of the total area of the eye diagram with the body channel noise. This finding reveals a satisfactory signal quality compared with 53% of the total area of the eye diagram without the body channel noise shown in Fig. 4(c). The typical waveform shows the high pass effect slightly deteriorates the signal quality in the experiment. According to this figure, a simple digital circuit design approach can easily implement the data recovery circuit following the front-end amplifier.

6. Conclusions

The direct transmission of digital signals in ESC intra-body communication can reduce the complexity of circuit design and the power consumption and improve the data rate of the system. This study develops a simplified bandpass channel circuit model to analyze the response of a high pass 3 dB pole of the system to a digital baseband signal. A wideband digital baseband signal can be transmitted directly through the human body with a good signal quality if the high pass 3 dB pole region is properly selected. The results of the experimentally implementation reveal a system data rate of 16 MBPS, an output voltage of 3.3 V and a transmitter power consumption of 560 μW.

Acknowledgment

The authors would like to thank the National Center for High-Performance Computing and the National Science Council of the Republic of China, Taiwan, R.O.C. under Grant NSC95-2221-E-009-334. Ted Knoy is appreciated for his editorial assistance.

References

[1] T.G. Zimmerman, "Personal area network: Near-field intrabody communication," IBM Syst. J., vol, no.3&4, pp.609–617, 1996.
[2] E.R. Post, M. Renolds, M. Gray, J. Paradiso, and N. Gershenfeld, "Intra-body bus for data and power," Proc. 1st international Symposium on Wearable Computers, IEEE Comp. Soc. Press, 1997.

[3] K. Hachisuka, A. Nakata, T. Takeda, Y. Terauchi, K. Shiba, K. Sasaki, H. Hosaka, and K. Itao, "Development and performance analysis of an Intra-body communication device," Tech. Digest, 12th Int. Conf. Solid-Stae Sens. Actuat. Microsystems, pp.1722–1725, Boston, MA, USA, June 2003.

[4] M. Shinagawa, M. Fukumoto, K. Ochiai, and H. Kyuragi, "A near-field-sensing transceiver for intrabody communication based on the electrooptic effect," IEEE Trans. Instrum. Meas., vol.53, no.6, pp.1533–1538, Dec. 2004.

[5] S.-J. Song, N. Cho, and H.-J. Yoo, "A 0.2-mW 2-Mb/s digital transceiver based on wideband signaling for human body communications," IEEE J. Solid-State Circuit, vol.42, no.9, pp.2021–2033, Sept. 2007.

[6] H. Kanai, I. Chatterjee, and O.P. Gandhi, "Human body impedance for electromagnetic hazard analysis in the VLF to MF band," IEEE Trans. Microw. Theory Tech., vol.MTT-32, no.8, pp.763–772, Aug. 1984.

[7] D.C. Barber and B.H. Brown, "Review article: Applied potential tomography," J. Phys. E, vol.12, pp.443–448, 1984.

[8] J.G. Webster, Electrical Impedance Tomography, Adam Hilger, New York, 1989.

[9] N.V. Thakor and J.G. Webster, "Ground-free ECG recording with two electrodes," IEEE Trans. Biomed. Eng., vol.BME-27, no.12, pp.699–704, Dec. 1980.

[10] J.G. Webster, Medical instrumentation: Application and design, Wiley, 1998.

[11] K. Hachisuka, A. Nakata, T. Takeda, Y. Terauchi, K. Shiba, K. Sasaki, H. Hosaka, and K. Itao, "Development and performance Analysis of an Intra-body communication device," Tech. Digest, 12th Int. Conf. Solid-Stae Sens. Actuat. Microsystems, pp.1722–1725, Boston, MA, USA, June 2003.

[12] K. Fujii, K. Ito, and S. Tajima, "A study on the calculation model for signal distribution of wearable devices using human body as a transmission channel," IEICE Trans. Commun. (Japanese Edition), vol.J87-B, no.9, pp.1383–1390, Sept. 2004.

[13] K. Fujii, M. Takahashi, K. Ito, K. Hachisuka, Y. Kishi, and K. Sasaki, "A study on the transmission mechanism for wearable device using the human body as a transmission channel," IEICE Trans. Commum., vol.E88-B, no.6, pp.2401–2410, June 2005.

[14] K. Hachisuka, Y. Terauchi, Y. Kishi, T. Hirota, K. Sasaki, H. Hosaka, and K. Ito, "Simplified circuit modeling fabrication of intrabody communication devices," Solid-State Sensors, Actuators and Microsystems, 2005. Digest of Technical Papers. TRANSDUCERS'05. The 13th International Conference on, vol.1, June 2005.

[15] IEC (International Electrotechnical Commission), "IEC 61000 ED. 1.2: Electromagnetic compatibility (EMC) — Part 4-2: Testing and measurement techniques — Electrostatic discharge immunity test," 2001.